Presented at the 22nd European Photovoltaic Solar Energy Conference
Milan, Italy, 3 September 2007

MILESTONES TOWARD 50% EFFICIENT SOLAR CELL MODULES

Allen Barnett[1], Douglas Kirkpatrick[2], Christiana Honsberg[1], Duncan Moore[4], Mark Wanlass[3], Keith Emery[3], Richard Schwartz[5], Dave Carlson[6], Stuart Bowden[1a], Dan Aiken[7], Allen Gray[7], Sarah Kurtz[3], Larry Kazmerski[3], Tom Moriarty[3], Myles Steiner[3], Jeffery Gray[5], Tom Davenport[8], Roger Buelow[9], Laszlo Takacs[9], Narkis Shatz[10], John Bortz[10], Omkar Jani[1,11], Keith Goossen[1], Fouad Kiamilev[1], Alan Doolittle[11], Ian Ferguson[11], [2], Blair Unger[4], Greg Schmidt[4], Eric Christensen[4], David Salzman[12]

[1]University of Delaware, Electrical and Computer Engineering, 201 Evans Hall, Newark, DE, USA 19716-3130
[1a]IEC, University of Delaware, [2]Defense Advanced Research Projects Agency (DARPA), [3]National Renewable Energy Laboratory (NREL), [4]University of Rochester, [5]Purdue University, [6]BP Solar , [7]Emcore Corporation, [8]Optical Research Associates, [9]Energy Focus, [10]Science Applications International Corporation (SAIC), [11]Georgia Institute of Technology, [12]LightSpin Technologies

ABSTRACT: The Very High Efficiency Solar Cell (VHESC) program is developing integrated optical system - PV modules for portable applications that operate at greater than 50 percent efficiency. We are integrating the optical design with the solar cell design, and have entered previously unoccupied design space. Our approach is driven by proven quantitative models for the solar cell design, the optical design and the integration of these designs. Optical systems efficiency with an optical efficiency of 93% and solar cell device results summing to 42.9% are described.
Keywords: High performance, module architecture, solar cell efficiency

1 INTRODUCTION

High efficiency modules are being developed based on the co-design of the optics, interconnects and solar cells. This architecture significantly increases the design space for high performance photovoltaic modules in terms of materials, device structures and manufacturing technology. It allows multiple benefits, including increased theoretical efficiency, new architectures which circumvent existing material/cost trade-offs, improved performance from non-ideal materials, device designs that can more closely approach ideal performance limits, reduced spectral mismatch losses and increased flexibility in material choices. An integrated optical/solar cell allows efficiency improvements while retaining low area costs, and hence expands the applications for photovoltaics. It allows a design approach which focuses first on performance, enabling the use of existing state-of-the-art photovoltaic technology to design high performance, low cost multiple junction III-Vs for the high and low energy photons and a new silicon solar cell for the mid-energy photons, all while circumventing existing cost drivers through novel solar cell architectures and optical elements.

2 PHOTOVOLTAIC SYSTEM ARCHITECTURE

The new system architecture is based on a “parallel” or lateral optical concentrating system, which splits the incident solar spectrum into several bands, and allows different optical and photovoltaic elements in each band. The optics and the cells are co-designed to achieve the maximum conversion efficiency of the module. An example of the photovoltaic system architecture is shown in Fig.1. The new architecture integrates optical and solar cell design, allowing a much broader choice of materials and circumventing of many existing cost drivers. This architecture enables the inclusion of multiple other innovations and leads to higher efficiency, both at solar cells and module level. The optical system consists of a tiled nonimaging concentrating system, coupled with a spectral splitter that divides the solar spectrum into a given number of bands.

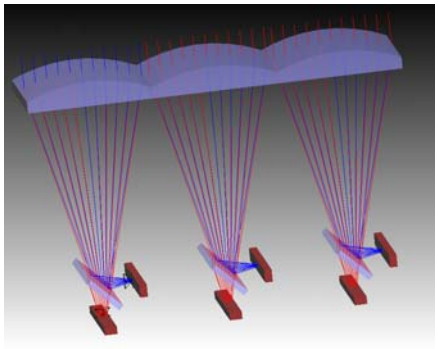

Figure 1: Schematic showing the optical elements in the lateral optics, including a static concentrator and spectral splitting.

2.1 Photovoltaic architecture

The lateral solar cell architecture increases the choice of materials for multiple junction solar cells, by allowing the solar cell in each spectral band to be optimized independently of the others. In this way, the lattice and current matching constraints are reduced. Further, since the devices do not need to be series connected, spectral mismatch losses are reduced, important for tandems in terrestrial environments. Finally, by contacting the individual solar cells with individual voltage busses, the need for tunnel junctions is avoided. Since each material requires unique tunnel contact metallurgy, eliminating tunnel junctions is a substantial simplification.

2.2 Lateral optical system

To achieve the benefits of the new PV system architecture, a new optical element is designed, which combines a nonimaging optical concentrator (which does not require tracking and is called a static concentrator) with spectral splitting approaches that split the light into several spectral bands. This system is called a parallel or lateral concentrator, since solar cells are not placed vertically or optically in series. These optical elements

are tiled, with the overall optical module being an affordable and manufacturable optical element, which incorporates both static concentration and a dichroic element for spectral splitting as shown in Figure 2.

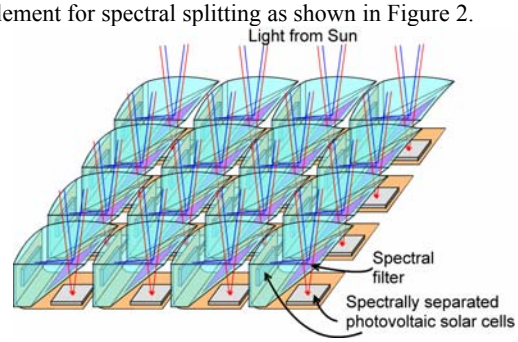

Figure 2: Schematic of the solar system architecture, which combines new optical elements.

The unique features of the optical system are an emphasis on high system optical efficiency, the use of dichroic mirrors for spectral splitting and the design of the system to be thin enough to allow integration with other products. For example, previous approaches of static concentrators have not been practical because the thickness of the optical elements is too large for conventional modules. Further, previous optical systems, particularly spectral splitters, have suffered from reduced optical efficiencies. The use of an integrated system and small area dichroic mirrors allows both the efficiency and cost issues to be overcome. The optical system does not require tracking and has no moving parts.

The critical metric for the module development is module efficiency. Module efficiency consists of two terms: (1) optical efficiency which is the amount of sunlight that is directed to the solar cells – weighted by the energy in each band of sunlight and (2) the sum of the power from each solar cell.

3 OPTICS DESIGN AND RESULTS

The optical design is based on non-symmetric, nonimaging optics, tiled into an array. The central issues in the optical system are the optical efficiency and the amount of time over which the sunlight remains focused on the solar cells (tracking time). Because the modules are designed for portable electronics, the concentrators are designed to accept light for several hours, rather than over the course of an entire day.

In order to make a system which has no moving parts and can work with maximum pointing error and maximum tracking time, proof of concept (POC) designs were created that consist of four components, as shown in Figure 3. These are: (1) a front lens array using non-spherical lenses (toroids or crossed cylinders); (2) a hollow pyramidal reflective concentrator array which increases the performance of the system for light which is not normal to the module; (3) a nonimaging solid concentrator on the solar cell converting photon energies between 2.4 eV and 1.4 eV (called mid-energy solar cells); and (4) a dichroic prism which reflects the light above 1.4 eV and passes light below this energy.

The fabricated POC has four unit cells arranged in a 2 x 2 array. In addition to the optical elements, the module contains a motherboard that holds the silicon chips, two daughterboards that hold the mid-E chips and a pair of aluminum spacers acting as heat sinks.

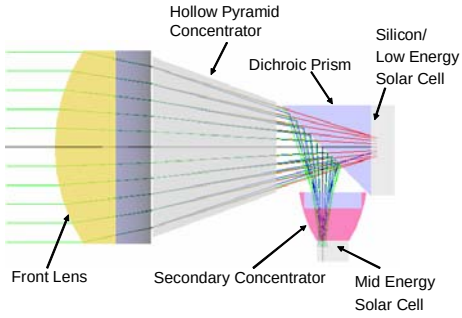

Figure 3: Schematic of the fabricated POC.

The front lens array sits on top of the pyramid concentrator array. Each of two dichroic prisms sit on top of two adjacent silicon chips, attached by means of an optical cement. The secondary concentrators are attached with optical cement to each of the mid-E chips. The aluminum spacers are then used to connect and align the pyramid concentrator array with the circuit board with the appropriate distance between the two components. The total thickness from the refractive lens to the motherboard is 11mm. The front lens array is made by diamond-turning plastic. The pyramid concentrator array and the secondary concentrators are molded plastic pieces. The dichroic prisms are made of BK7 glass. Fig. 4 is a picture of the assembled prototype.

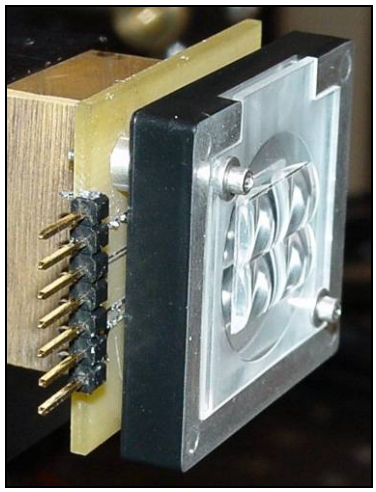

Figure 4: Assembled Crossed Cylinders POC

The transmission efficiency of the optical system was determined by measuring the reflectivity and transmission for all AR coatings, the material absorption for the optical elements and dichroic coatings. Using this data in a commercial optical design software shows that the optical transmission under weighted average AM1.5G spectrum is greater than 93%. Further, since the manufacturing tolerances of the optical components are an order of magnitude lower than for other optical systems, the dominant loss is the reflectivity and transmission. Thus overall, the optical system has a weighted average efficiency of >93% under AM1.5G. The results are shown in Figure 5.

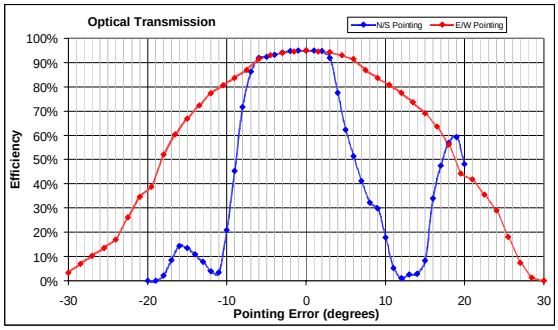

Figure 5: Optical transmission as a function of angle away from normal to the module.

Since the module is designed for portable battery charging applications, the time in which the module is stationary is relatively short. The tracking time or field of view is limited by the size of the photovoltaic cells and "beam walk" or the tendency of the spot of energy on the detector to move as the angle of the sun changes. Experiments were performed to measure the efficiency of the POC prototype as a function of the pointing error, i.e., the efficiency of the system when it is not aimed directly at the sun. These measurements were made in the lab using the solar simulator with an 18.3 mm diameter aperture in front of the focusing element. Figure 6 shows the efficiency of the total system for off-axis pointing in the East/West direction.

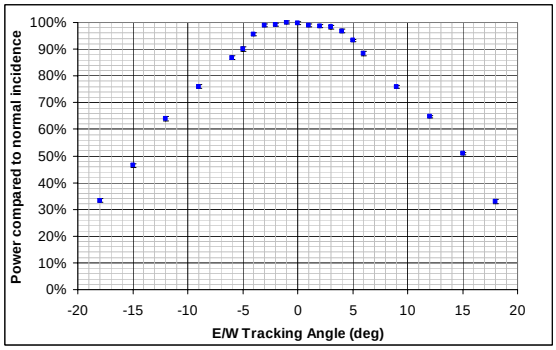

Figure 6: Performance of the POC with East/West tracking angle.

4 EFFICIENCY MEASUREMENT METHOD

The efficiency of a concentrator cell is usually measured without regard to the design or performance of the optics [1]. The efficiency of a lens-cell assembly reflects both the optical and cell efficiencies. No standard exists for characterization of the performance of a collection of concentrator cells designed for use under optics that split the spectrum into two or more parts. Consensus standards currently use a global reference spectrum for flat-plate measurements and a direct reference spectrum for concentrator measurements, but a reference spectrum for a low-concentration application has not been defined. Thus, cell performance measurements for the new PV architecture require two new elements: (1) definition of the spectrum relevant to this low concentration application and (2) identification of a methodology for quoting an aggregate efficiency for a set of cells that each use a different portion of the spectrum. These two issues have been addressed by (1) choice of the AM1.5 Global spectrum [2], and (2) the solar spectrum being split, mathematically, either by defining dividing wavelengths or by any other method, such that the spectral parts sum to give the one-sun reference spectrum. Each cell is then measured in the conventional way using the portion of the spectrum assigned to it. For the results presented here, the spectrum was divided into three sections with the GaInP/GaAs cell measured above the GaAs response (roughly 900 nm), the GaInAsP/GaInAs cell with light beyond 1100 nm and the silicon from 900 to 1100 nm. The solar cells are measured over a range of concentrations, but the VHESC Program reporting conditions were taken as 20 suns.

The quantitative performance measurement of each individual solar cell uses reference cells to characterize the intensity of the solar simulator and a spectral mismatch correction factor to correct for differences between the test and reference cell responses and differences between the test and mathematically calculated reference spectrum relevant to that cell.

The most difficult measurement is for the low-band-gap series-connected tandem solar cell. Accurate measurement of this cell requires adjustment of the incident spectrum so that each of the junctions generates the correct photocurrent. Multi-source simulators provide a means for obtaining the desired spectrum, but today's multi-source simulators do not achieve the concentrations desired for this project. Separate electrical contacts made this device easier to fabricate and measure. Detailed description of the measurement conditions have been previously given [3].

5 SOLAR CELL DESIGNS AND RESULTS

The central approach in choosing among the expanded material design space allowed by the optical elements is to first design for performance, eliminating only those aspects fundamentally incompatible with ultimately achieving low cost and then design for low cost manufacture. This approach involves parallel approaches in the initial phases, such that success in no case depends on a single approach.

The increased design space provides a path to circumventing lattice and current matching constraints imposed by monolithic, series connected tandems. For lattice-matched (or close to lattice-matched metamorphic) tandems, only a limited number of materials are available. However, in the lateral optical approach, the materials can be chosen for their performance potential. This is particularly important for the very high energy band gaps required for the 5 and 6 junction tandems.

The design emphasis on high performance leads to a core approach based on using materials that have demonstrated the highest performance for the wavelength range close to their band gap. For the solar cells with band gaps in the range of 1.4 and 1.9 eV, the highest performance materials are ternary compounds from the GaInAsP materials system [4,5,6,7] with silicon being the highest performing material for the photons [8,9] with energy near 1.0 eV. The optimum band gaps, and in some cases materials for the proposed solar cell, are shown in Fig. 7. Included are de-rating factors to account for unavoidable losses such as parasitic resistances and reflection. The proposed six junction solar cell, including the de-rating factors, can achieve and efficiency of 54% at 20X. When coupled with an optical system in excess of 93%, the system shows an ***overall system*** efficiency,

not just the solar cell efficiency, of 50%.

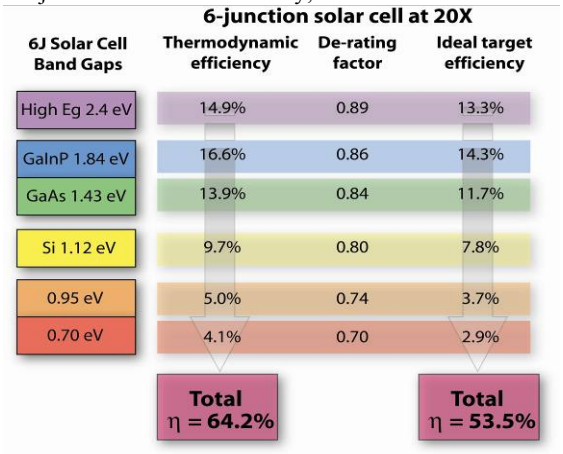

Figure 7: Predicted contributions of each solar cell in the proposed 6 junction design.

5.1 InGaN Solar Cells

The III-nitride material system has several features that allow both high performance multi-junction solar cells and low cost. These features include: an existing industry centered around the nitrides; high radiative efficiency even with high dislocation densities [10]; high mobilities, allowing good collection; a large piezoelectric constant, allowing control of surface recombination [11,12]; and the availability of direct high band gap materials, with band gaps above 2.4 eV. Such high band gaps are not available in other established material systems, but are necessary for multiple junction solar cells with a large number of cells. Coupled with these advantages are also substantial challenges. These include the difficulty in achieving p-type conduction in material with 2.4 eV or below [13]), and phase separation in material with higher concentrations of indium leading to increased recombination.

We experimentally demonstrated the III-V nitrides as a high-performance photovoltaic material with a Voc of 2.4V and an IQE as high as 60%. GaN and high-band gap InGaN solar cells are designed using modified PC1D software [14], grown by standard industrial MOCVD, fabricated into devices of variable sizes and contact configurations and characterized for material quality and performance. The material is primarily characterized by X-ray diffraction and photoluminescence to understand the implications of crystalline imperfections on photovoltaic performance. Phase separation within the material and high-contact resistances are identified as the two major efficiency loss mechanisms.

The design of the III-nitride solar cell consists of a lower-band gap InGaN region sandwiched between the top p- and the supporting n-type GaN junctions. A typical I-V curve of a high band gap solar cell (~3.0 eV or greater) is shown in Figure 8. The light source used is modified from a typical one-sun spectrum by increasing its UV content to amplify the response of the solar cell. The open-circuit voltage (Voc) of the solar cell is dominated by the lower band gap phase separated InGaN. A central challenge in these devices is the formation of a Schottky barrier at the non-optimal p-GaN – Ni metal contact interface, which opposes the light-generated current so that the current asymptotically approaches zero prior to the device reaching its V_{OC}; this Schottky effect is also confirmed through PC1D simulation. These effects mean that existing devices have a semi-transparent current spreading layer consisting of full metal coverage on the top of the solar cell. In spite of the relatively lower short-circuit currents (Jsc) due to light absorption by the top current spreading layer, the full-metal contacts with p-GaN yield lower series resistance around 30-50Ω. These solar cells demonstrate Voc's as high as 2.4V and fill factors (FF) about 78%.

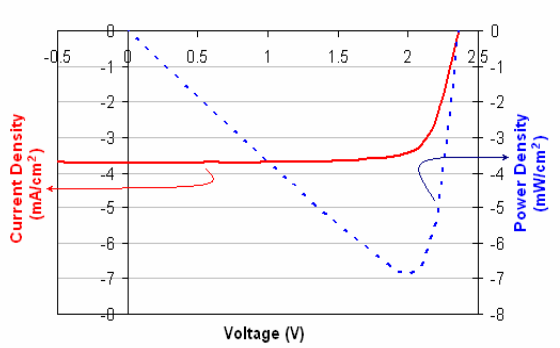

Figure 8: Typical I-V curve for a GaN/InGaN solar cell with semi-transparent p-contact metal.

5.2 GaInP/GaAs Solar Cells

A viable path to increased efficiency for multi-junction monolithic solar cells is to independently optimize the voltage and current production of each cell to the solar spectrum. Solar cell modeling has shown that the independently interconnected or multi-terminal design is not constrained by minimum cell current and is less sensitive to bandgap as compared to series connected solar cell designs. However, it is more complex with respect to fabrication of the solar cell, and in terms of power delivery. The I-V curve of the best GaInP/GaAs tandem solar cell is shown in Figure 9.

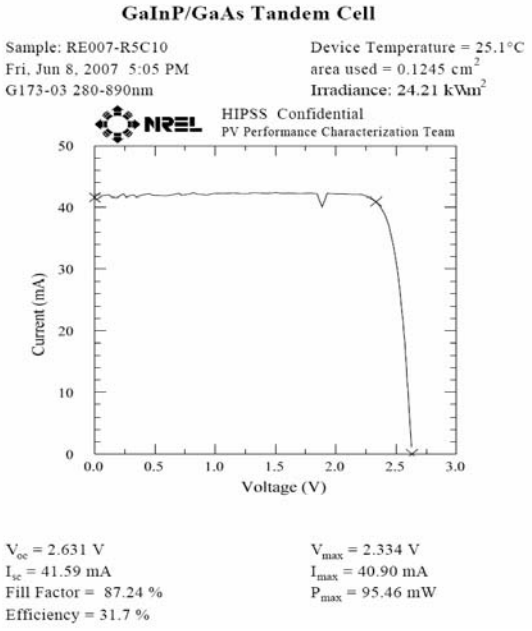

Figure 9: I-V curve of the best GaInP/GaAs solar cell at 20X. This solar cell was fabricated by Emcore.

5.3 Silicon Solar Cell filtered by GaAs

A central feature of our proposed approach is to leverage the cost/performance benefits of existing solar cell technology to achieve both high performance and low risk. While laboratory silicon solar cells have

demonstrated high performance, a central challenge is to incorporate the high performance features in a low cost solar cell. Several innovations in solar cell design make this possible, including the move to thinner silicon junctions, the passivation of Si surfaces by means other than insulators [15], the use of an optically transparent substrate and recently demonstrated high minority carrier lifetimes in n-type silicon. Silicon solar cells were fabricated using the deposition of the wide-band gap semiconductor, amorphous silicon to passivate the surfaces and achieve higher voltages and efficiencies.

The device structure is a heterojunction between crystalline silicon and amorphous silicon, thereby utilizing the excellent passivation by the amorphous silicon to reduce recombination and maximize efficiency. Silicon heterojunction solar cells are ideally suited to the VHESC program since the III-V based top cell removes short wavelength light where the absorption in the amorphous silicon window layer is otherwise a problem, and the effective concentration of 5 – 6 suns shifts the operating point away from the high ideality factor region experienced by the one sun cells [16].

The cell design is pictured in Fig. 10. The center section in blue is the active area (8 mm x 2 mm) of the cell and is transparent to below bandgap infrared light. The outer section in red is the metallization for the contacts. The cell dimensions are small enough to allow conduction along the TCO, and through the cell bulk, with minimal resistance losses. The best filtered results at 20X are shown in Fig 11.

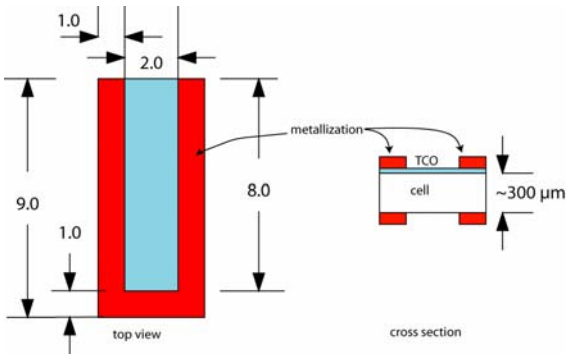

Figure 10: Cell design in mm. Metallization masks have been fabricated to these dimensions.

5.3 GaInAsP/GaInAs bottom tandem cells.

The low band gap solar cells consist of two independently connected (3 terminals) GaInAsP/GaInAs solar cells. The 3-terminal approach for the monolithic bottom tandem solar cell allowed measurement of the performance of each subcell in the tandem structure independently, substantially simplifying the performance characterization. Since the subcells are not serially connected, a tunnel junction is not included in the tandem structure, which simplifies the growth procedure. The increased flexibility, better characterization and simplified structure allow a high efficiency subcell. This in turn allows an increase of efficiency by lowering the band gap of the lowest energy subcell. A tandem device with subcell band gaps of 0.92 eV and 0.69 eV has been demonstrated with an efficiency of 6.2% at 20 suns under an idealized Si filter (1100 nm cutoff), global spectrum at 25 °C.

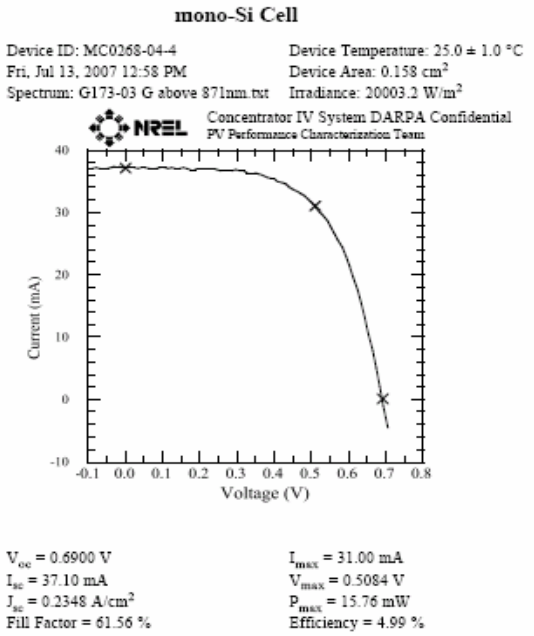

Figure 11: Best silicon solar cell under idealized GaAs filter at 20X This solar cell was fabricated by the University of Delaware.

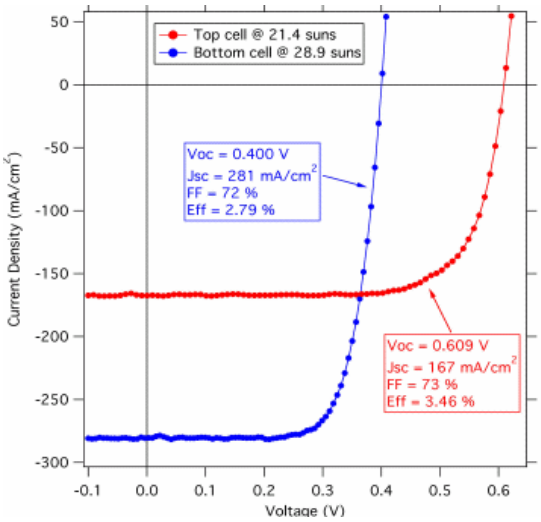

Figure 12: IV data for the top and bottom subcells of a 3-terminal GaInAsP/GaInAs tandem cell near 20 suns X under an idealized Si filter. The combined efficiencies of the subcells is 6.2%. This solar cell was fabricated by the National Renewable Energy Laboratory (NREL)

5.5 Sum of the solar cell efficiencies

The sum of the solar cell efficiencies, as described in Section 4 Efficiency Measurement method, gives the overall efficiency of the PV devices. These efficiencies are summarized below:

GaInP/GaAs = 31.7%
Silicon (filtered by GaAs) = 5%
GaInAsP/GaInAs (filtered by Si) = 6.2%
TOTAL = 42.9%

These results demonstrate the potential of the integrated optical approach, which allows a greater range of materials, and hence a larger number of band gaps. These devices represent a substantial increase in efficiency over existing tandem approaches [17,18] particularly given that the results are measured at 20X

rather than at high concentration typical of tandem devices.

6. CONCLUSIONS AND NEXT STEPS

The results of 93% optical efficiency combined with the 42.9% sum of the solar cell efficiencies are a good indication of the power of the new PV architecture. The next steps are to combine them into a module, improve the performance of the module, implement power conversion circuitry and transfer to production. The Watt-hours delivered to the battery need to be optimized.

The power of the collaborative approach is demonstrated by the number and breadth of organizations that contributed to the new architectural design and implementation. The optics designs included contributions from government, universities and industrial participants. The system reported here features three types of solar cells (5 junctions) —one made by industry, one by a Government Lab and one by a University. The continued development of this co-design approach to the optics interconnects and solar cells will lead to 50% efficient modules.

Acknowledgements

The research reported in this document was prepared through participation in an Agreement sponsored by the Government under DARPA/ARO Agreement W911NF-05-9-0005. James Kiehl, NREL also did some of the measurements. Dr. Dan Laubacher, DuPont, provided valuable assistance.

REFERENCES

[1] K. Emery, M. Meusel, R. Beckert, F. Dimroth, A. Bett and W. Warta, "Procedures for Evaluating Multijunction Concentrators," *Proc. 28th IEEE Photovoltaic Specialists Conf.*, Anchorage, AL, Sept. 2000, pp. 1126-1130, IEEE, New York, 2000.)

[2] ASTM Standard G173, "Standard Tables for Reference Solar Spectral Irradiances: Direct Normal and Hemispherical on 37° Tilted Surface," Amer. Society for Testing Matls., West Conshocken PA, USA

[3] A. Barnett, C. Honsberg, D. Kirkpatrick, S. Kurtz, D. Moore, D. Salzman, R. Schwartz, J. Gray, S. Bowden, K. Goosen, M. Haney, D. Aiken, M. Wanlass, K. Emery, T. Moriarty, J. Kiehl, "50% Efficient Solar Cell Architectures and Designs", *4th World Photovoltaic Science and Energy Conference*, Hawaii, USA, 2006.

[4] R.R King, S. Kurtz, P.C. Colter, D.E. Joslin, K.M. Edmondson, D.D. Krut, and N.H. Karam, "High-voltage, low-current GaInP/GaInP/GaAs/GaInNAs/Ge solar cells," *Proc. IEEE Photovoltaic Specialists Conference*, p. 852-855, (2002).

[5] R.R. King, C.M. Fetzer, P.C. Colter, K.M. Edmondson, D.C. Law, A.P. Stavrides, H. Yoon, G.S. Kinsey, H.L. Cotal, J.H. Ermer, R.A. Sherif, K. Emery, W. Metzger, R.K. Ahrenkiel, and N.H. Karam, "Lattice-matched and metamorphic GaInP/GaInAs/Ge concentrator solar cells," *Proc 3rd World Conference on Photovoltaic Energy Conversion*, 622-625, (2003).

[6] F. Dimroth, R. Beckert, M. Meusel, U. Schubert, and A.W. Bett, "Metamorphic $Ga_yIn_{1-y}P/Ga_{1-x}In_xAs$ tandem solar cells for space and for terrestrial concentrator applications at C>1000 suns," *Progress in Photovoltaics: Research and Applications*, vol. 9, no. 3, p. 165-78, (2001).

[7] M. Yamaguchi, T. Takamoto, A. Khan, M. Imaizumi, S. Matsuda, and N.J. Ekins-Daukes, "Super-high-efficiency multi-junction solar cells," *Progress in Photovoltaics*, vol. 13, no. 2, p. 125-132, (2005).

[8] Martin A. Green, J. Zhao, A. Wang, and S. R. Wenham, "45% efficient silicon photovoltaic cell under monochromatic light," *IEEE Electron Device Letters*, vol. 13, no. 6, p. 317-318, (1992).

[9] A. Wang, M. Green, J. Zhao, "24.5% efficiency silicon PERT cells on MCZ substrates and 24.7% efficiency PERL cells on FZ substrates," *Progress in Photovoltaics:* vol. 7, no. 6, p. 471-474, (1999).

[10] O. Brandt, H.-J. Wünsche, H. Yang, R. Klann, J.R. Müllhäuser, and K.H. Ploog, "Recombination dynamics in GaN," *Journal of Crystal Growth*, vol. 189/190, p. 790-793, (1998).

[11] Robert D. Underwood, P. Kozodoy, S. Keller, S.P. DenBaars, and U.K. Mishra, "Piezoelectric surface barrier lowering applied to InGaN/GaN field emitter arrays," *Applied Physics Letters*, 73, 3, 405, (1998).

[12] J.R. Shealy, T.R. Prunty, E.M. Chumbes, and B.K. Ridley, "Growth and passivation of AlGaN/GaN heterostructures," *Journal of Crystal Growth*, vol. 250, no. 1, p. 7-13, (2003).

[13] W. Walukiewicz, S.X. Li, J. Wu, K.M. Yu, J.W. Ager III, E.E. Haller, and Hai, Schaff, William J. Lu, "Optical properties and electronic structure of InN and In-rich group III-nitride alloys," *Journal of Crystal Growth*, vol. 269, no. 119, p. 119-127, (2004).

[14] P. A. Basore, D. A. Clugston, PC1d Version 5.9, Sydney, Australia: Univ. New South Wales, 2003.

[15] M. Taguchi, K. Kawamoto, S. Tsuge, T. Baba, H. Sakata, M. Morizane, K. Uchihashi, N. Nakamura, S. Kiyama and O. Oota, "HIT Cells – High Efficiency Crystalline Si Cells with Novel Structure", *Progress In Photovoltaics,* Vol 8 p. 503-513 (2000)

[16] M. D. Lammert, R. J. Schwartz, IEEE Trans. Electron Devices, 24, 337 (1977)

[17] R. R. King, D. C. Law, C. M. Fetzer, R. A. Sherif, K. M. Edmondson, S. Kurtz, G. S. Kinsey, H. L. Cotal, D. D. Krut, J. H. Ermer, and N. H. Karam, *Proc. 20th European Photovoltaic Solar Energy Conf.* (Barcelona, Spain, June, 2005), p. 118.

[18] M. Green, K. Emery, K. D.L King, Y. Hisikawa, and W. Warta, "Solar cell efficiency tables (Version 27)", *Progress in Photovoltaics*, 14, 1, 45-51 (2006).